

THIS IS A COPY

4

ERL-0473-TR

AR-005-879



AD-A214 531

DEPARTMENT OF DEFENCE
DEFENCE SCIENCE AND TECHNOLOGY ORGANISATION
SALISBURY
ELECTRONICS RESEARCH LABORATORY
SOUTH AUSTRALIA

TECHNICAL REPORT
ERL-0473-TR

A STATISTICAL MODEL OF THE INFRARED SIGNATURE OF A WIND ROUGHENED SEA

S.A. BRUNKER and G. HAMLYN

DTIC
ELECTE
NOV 24 1989
S B D

Approved for Public Release

C Commonwealth of Australia
March 1989

89 11 21 045

THE UNITED STATES NATIONAL
TECHNICAL INFORMATION SERVICE
IS AUTHORISED TO
REPRODUCE AND SELL THIS REPORT

CONDITIONS OF RELEASE AND DISPOSAL

This document is the property of the Australian Government. The information it contains is released for defence purposes only and must not be disseminated beyond the stated distribution without prior approval.

Delimitation is only with the specific approval of the Releasing Authority as given in the Secondary Distribution statement.

This information may be subject to privately owned rights.

The officer in possession of this document is responsible for its safe custody. When no longer required the document should NOT BE DESTROYED but returned to the Main Library, DSTO, Salisbury, South Australia.

UNCLASSIFIED

AR-005-879

DEPARTMENT OF DEFENCE

DEFENCE SCIENCE AND TECHNOLOGY ORGANISATION

ELECTRONICS RESEARCH LABORATORY

TECHNICAL REPORT

ERL-0473-TR

A STATISTICAL MODEL OF THE INFRARED SIGNATURE OF A WIND ROUGHENED SEA

S.A. Brunker and G. Hamlyn

SUMMARY

The response of any Optical System, used in either a weapon or surveillance mode, is dependent upon the emission of electromagnetic energy from both target and background occupying the field of view. The background not only contributes to the infrared scene (clutter) but, additionally, by reflection and absorption, can significantly contribute to the target's signature.

Since the maritime environment can be conceived as containing an opaque homogeneous body of water, its signature will depend upon the predictable behaviour of such a surface in response to the natural elements.

This report proposes a statistical-numerical method which can be used to obtain the infrared signature of both a calm and wind roughened sea in the 1 to 15 μm waveband.

POSTAL ADDRESS: Director, Electronics Research Laboratory,
PO Box 1600, Salisbury, South Australia 5108

UNCLASSIFIED

TABLE OF CONTENTS

	Page
1. INTRODUCTION	1
2. RADIANCE MODEL	1
2.1 Calm sea	1
2.2 Wind roughened sea	2
2.2.1 Shadowing	3
2.2.2 Multiple scattering	4
3. INTEGRAL EVALUATION	4
4. RESULTS AND DISCUSSIONS	8
4.1 Long waveband	8
4.2 Short waveband	8
4.3 Image representation	9
4.4 Irradiance	14
5. CONCLUSION	20
6. ACKNOWLEDGEMENTS	21
REFERENCES	22
TABLE 1. COMPARATIVE VARIATION IN SEA RADIANCE VALUES	11



LIST OF FIGURES

- 1. Geometry for reflection angles from a sea surface facet
- 2(a). Flow diagram of radiance model main program
- 2(b). Flow diagram of subroutine rough
- 3(a). Comparative LWB sea radiance profiles

Accession For	
NTIS GRA&I	<input checked="" type="checkbox"/>
DTIC TAB	<input type="checkbox"/>
Unannounced	<input type="checkbox"/>
Justification	
By _____	
Distribution/	
Availability Codes	
Dist	Avail and/or Special
A-1	

- 2
- 6
- 7
- 9

3(b). Comparative LWB sea/sky radiance profiles	9
4(a). Mean radiance against refractive index for $\delta = 0.1$	10
4(b). Mean radiance against refractive index for $\delta = 0.3$	10
5. Elevation as a function of mean sky radiance SWB	11
6(a). SWB sea/sky radiance profile for 180° azimuth angle from sun	13
6(b). SWB sea/sky radiance profile for same sun azimuth angle	13
7. SWB sea/sky radiance profile for different azimuth angles	14
8. Numerical generation of (LWB) 8 to 12 μm images of the maritime scene	16
9. Numerical generation of LWB and (SWB) 3 to 4 μm images of the maritime scene	17
10. Geometry of observer relative to the Earth horizon coordinate system	18
11. L_2 as a function of viewing angle	19
12. Vertical height as a function of viewing angle	20

LIST OF APPENDICES

I REFLECTED ANGLE DETERMINATION	23
Figure I.1 Wave facet as tangent plane	25
II SEA RADIANCE INTEGRAL EVALUATION	26

1. INTRODUCTION

To determine the response of any optical system (weapon or surveillance) to the electromagnetic emission of a target under consideration, it is often necessary to have knowledge of the target's background. The background can not only contribute directly to the scene (clutter) but additionally by interaction with the target it can contribute significantly to the target's signature.

The maritime environment, as a background scene, can be conceived as a homogeneous body of water that responds to the natural elements in a predictable manner. Because of such behaviour the maritime environment conveniently offers itself to be mathematically modelled such that within the 1 to 14 μm waveband its infrared signature can be determined.

Two approaches can be used to model the maritime environment. The first is a statistical model which was developed by Saunders(ref.1) to predict the radiance of the sea in the 12 to 14 μm waveband. The second approach is a method used to predict the sea's infrared signature by a geometrical interpretation of the sea surface. This method offers both a spatial and time variant infrared scene of a calm and wind roughened sea. Although this approach may seem to have a definite advantage over that of a static statistical surface, if the radiance of the sea is needed over a large portion of the surface (many wave periods) then the computing time necessary to evaluate such, can become both timely and costly. This situation can arise when an imager for example contains a wide field of view or when a narrow field of view is used at an extended range from a region of the sea surface. Such a model will be discussed in another report(ref.2).

The following report discusses the statistical approach used to predict the signature of both a calm and wind roughened sea. It combines the method of Cox and Munk(ref.3) and that of Saunders to form the basis onto which a numerical method is developed, to produce a signature over the entire 1 to 15 μm waveband.

2. RADIANCE MODEL

The signature of the sea surface in the 8 to 12 μm waveband is well documented and has been treated by several authors. The requirement is to supplement and expand on such models to include the shorter wavebands so that the usable range extends from 1 to 14 μm . The difficulty encountered using shorter wavelength regions, is that the reflected radiation from the sea surface which originates from the sky significantly becomes a function of azimuth in addition to elevation, whereas the sky radiance in the longer 8 to 12 μm waveband is usually treated as only a function of elevation. The azimuth dependence must be accounted for and is detailed in the following model description.

2.1 Calm sea

The statistical model closely follows the approach taken by Saunders such that if (B) represents the Black Body radiance of the sea and (NS) represents the radiance of the sky, then at observation angle ϕ (see figure 1) the total radiance of a calm sea is given by

$$N = (B - R(B - NS)) \quad (1)$$

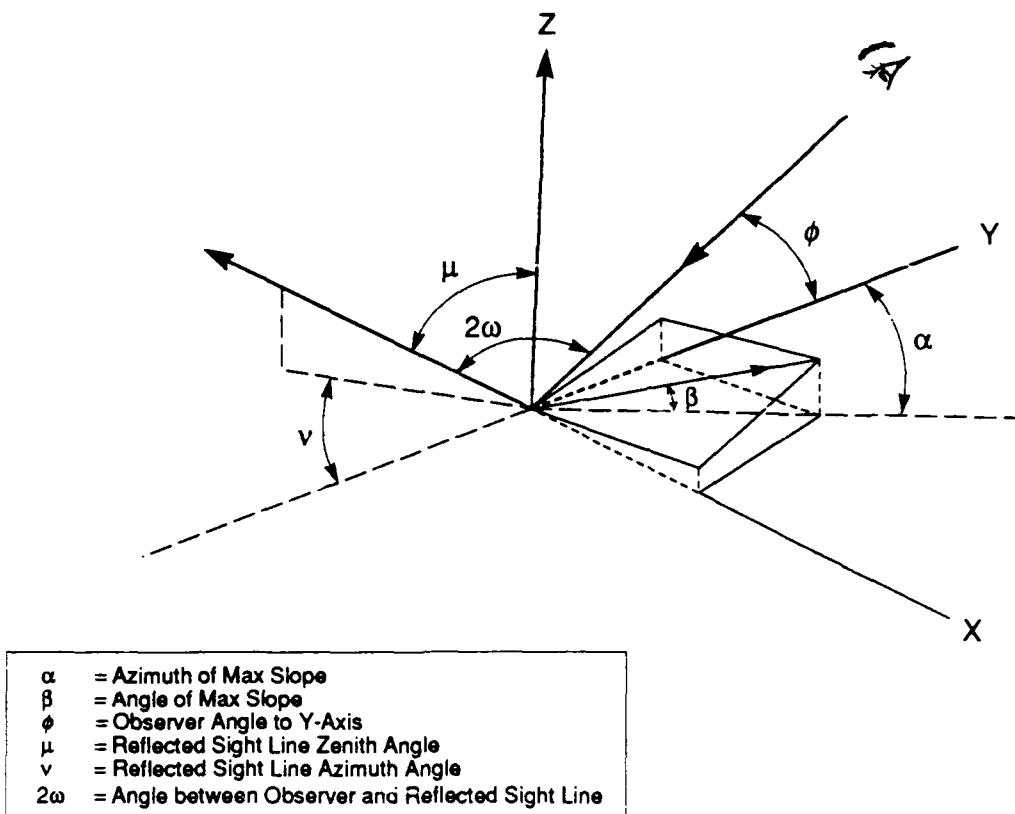


Figure 1. Geometry for reflection angles from a sea surface facet

where R is the reflectance for the sea and is calculated from the standard Fresnel equation

$$2 R(\omega) = \sin^2 (\omega' - \epsilon') \csc^2 (\omega' + \epsilon') + \tan^2 (\omega' - \epsilon') \cot^2 (\omega' + \epsilon')$$

where ω' and ϵ' are the incidence and transmittance angles respectively.

2.2 Wind roughened sea

In the presence of wind, equation (1) has to be modified to account for the waves of the sea which, for a given 'look down angle' (ϕ), will reflect portions of the sky extending over the entire hemisphere. That is, if $\phi = 0$ corresponds to looking at the horizon, then for $\phi = 80^\circ$ (that portion of sea below the observer) there is a finite probability that in the presence of waves there will be a contribution of sky radiance from the horizon albeit small. Because a probability or probability distribution is used, the resulting sea radiance is a time average of the instantaneous radiance.

The wave slope-distribution function $p(Z_x, Z_y)$ (ref.3) is defined as the probability of slope components Z_x, Z_y occurring in a unit area of horizontal sea surface. Thus $p(Z_x, Z_y) \delta Z_x \delta Z_y$ represents the fraction of surface with slope components in the interval $Z_x \pm \delta Z_x/2$ and $Z_y \pm \delta Z_y/2$ and equation (1) becomes

$$N = \operatorname{cosec} \phi \int \int (B - R [B - NS]) \cos \omega \sec \beta p(Z_x, Z_y) dZ_x dZ_y \quad (2)$$

where by referring to figure 1 and Appendix I, and for a look down angle ϕ , α , β , ω , μ and ν can be determined. Z_x and Z_y are the slope components in the X and Y directions respectively. The term $\operatorname{cosec} \phi$ is included as a constant for a given look down angle on the right hand side of equation (2) so that N becomes the radiance with respect to line of sight.

To account for the dependence of radiance on the azimuth direction (ν), equation (2) becomes

$$N(\phi) = S \operatorname{cosec} \phi \int_{-\infty}^{\infty} \int_{-\infty}^{\tan \phi} (B - R [B - NS(\mu, \nu)]) \cos \omega \sec \beta p(Z_x, Z_y) dZ_x dZ_y \quad (3)$$

The factor (S) in equation (3) is used to account for the reduction in the radiance due to the effects of both shadowing and multiple reflections. The finite integration limit, $\tan \phi$, accounts for including only those slope components which do not exceed the inclination of the line of sight.

2.2.1 Shadowing

The derivation and discussions of the slope-shadowing factor can be found in detail elsewhere(ref.1), accordingly it is sufficient to only provide the expression for S which accounts for the fraction of the surface which remains hidden from the line of sight due to the masking of waves by other waves closer to the observer. S is related to the error function and is given by

$$S = 2 \{1 + \operatorname{erf}(V) + (V\sqrt{\pi})^{-1} \exp - V^2\}^{-1}$$

where $V = \delta^{-1} \tan \phi$ and δ is the root mean square slope, the value which is obtained by the expression(ref.3)

$$\delta^2 = 0.003 + 5.12 \times 10^{-3} W$$

W is the wind velocity in ms^{-1} . To a first order the slopes of the sea surface are normally distributed and independent of wind direction thus the wave slope distribution function is related to the wind speed by the following expression

$$p(Z_x, Z_y) = (\pi\delta^2)^{-1} \exp\left[-\left(\frac{Z_x^2 + Z_y^2}{\delta^2}\right)\right]$$

The statistical sea radiance equation (3) does depend on wind speed but not wind direction.

2.2.2 Multiple scattering

Multiple scattering arises when the ray of electromagnetic radiation travelling towards the observer has undergone at least two reflections. This condition occurs when the elevation angle μ in figure 1 has the property

$$\mu \geq 90^\circ$$

that is the ray reflected toward the observer does so by a reflection such that the incident ray originates from below the horizon.

Multiple scattering is handled iteratively in the following report by a "Successive approximation" method which can be described by the following. Sea radiance values are first calculated for both normal and grazing viewing angles. This provides two boundary values such that the contribution of radiance from multiple scattering is calculated initially by interpolation between these boundaries resulting in the determination of the total sea radiance from a point just below the grazing viewing angle of the horizon. Having now three points to the sea radiance, the next radiance value can be determined by appropriately linearly interpolating. In such a manner each point of radiance is determined for angles progressively lower than the grazing viewing angle and toward the normal viewing angle. Thus the iterative technique builds up the sea radiance map, starting from the horizon and progressively determining points of radiance towards the normal viewing angle.

The effect of using a boundary at grazing viewing angle which was either too large or too small in calculating the second sea radiance value, was checked by deliberately using the largest possible radiance value and recording the sea radiance, and then the smallest possible radiance value (the Zenith radiance) and recording the value. The difference was found to be less than 1%.

3. INTEGRAL ELEVATION

Equation (3) cannot be easily analytically integrated. It was therefore necessary to numerically evaluate the integrals. With the appropriate change of variables (Appendix II) equation (3) reduces to the form

$$N(\phi, \theta) = k [I_1 + I_2] \quad (4)$$

where

$$I_1 = \delta^2 \int_{-\infty}^{\infty} \left[\int_0^{\infty} G(i, \psi) e^{-\psi} d\psi \right] e^{-\gamma^2} d\gamma \quad (5)$$

The inner integral can be evaluated using Gauss-Laguerre Quadrature and if we denote the evaluation of the inner integral as $H'(\gamma)$ then equation (5) reduces to

$$I_1 = \delta^2 \int_{-\infty}^{\infty} H'(\gamma) e^{-\gamma^2} d\gamma \quad (6)$$

which is in a form suitable to be evaluated by Gauss-Hermite Quadrature.

By a further manipulation in terms, the second integral in equation (4) can be reduced to

$$I_2 = \delta^2 \int_{-\infty}^{\infty} \epsilon \left[\int_{-1}^1 F(\delta\gamma, \delta(\epsilon + \rho\epsilon)) e^{-\epsilon^2(1+\rho)^2} d\rho \right] e^{-\gamma^2} d\gamma$$

Again the inner integral can be evaluated using Gauss-Legendre Quadrature and representing the evaluation by $M(\gamma)$, I_2 reduces to

$$I_2 = \delta^2 \int_{-\infty}^{\infty} M(\gamma) e^{-\gamma^2} d\gamma$$

which is of the form of equation (6) and can be similarly evaluated.

As discussed earlier, to evaluate equation (4) to account for any waveband then rather than evaluating the sky radiance $NS(\mu, \nu)$ semi empirically, the radiance information is read from a data file which contains values for the whole hemispherical sky. Values which are needed between the data file data points, are found by interpolation of the data set. At present it has been sufficient to use only linear interpolation.

The additional advantage of using such a file-reading technique is that experimentally measured data sets of sky radiance values can be entered if they are available. A flow diagram is shown in figure 2 to obtain the total sea radiance given wind velocity, azimuth of the observer and the sky-radiance data file.

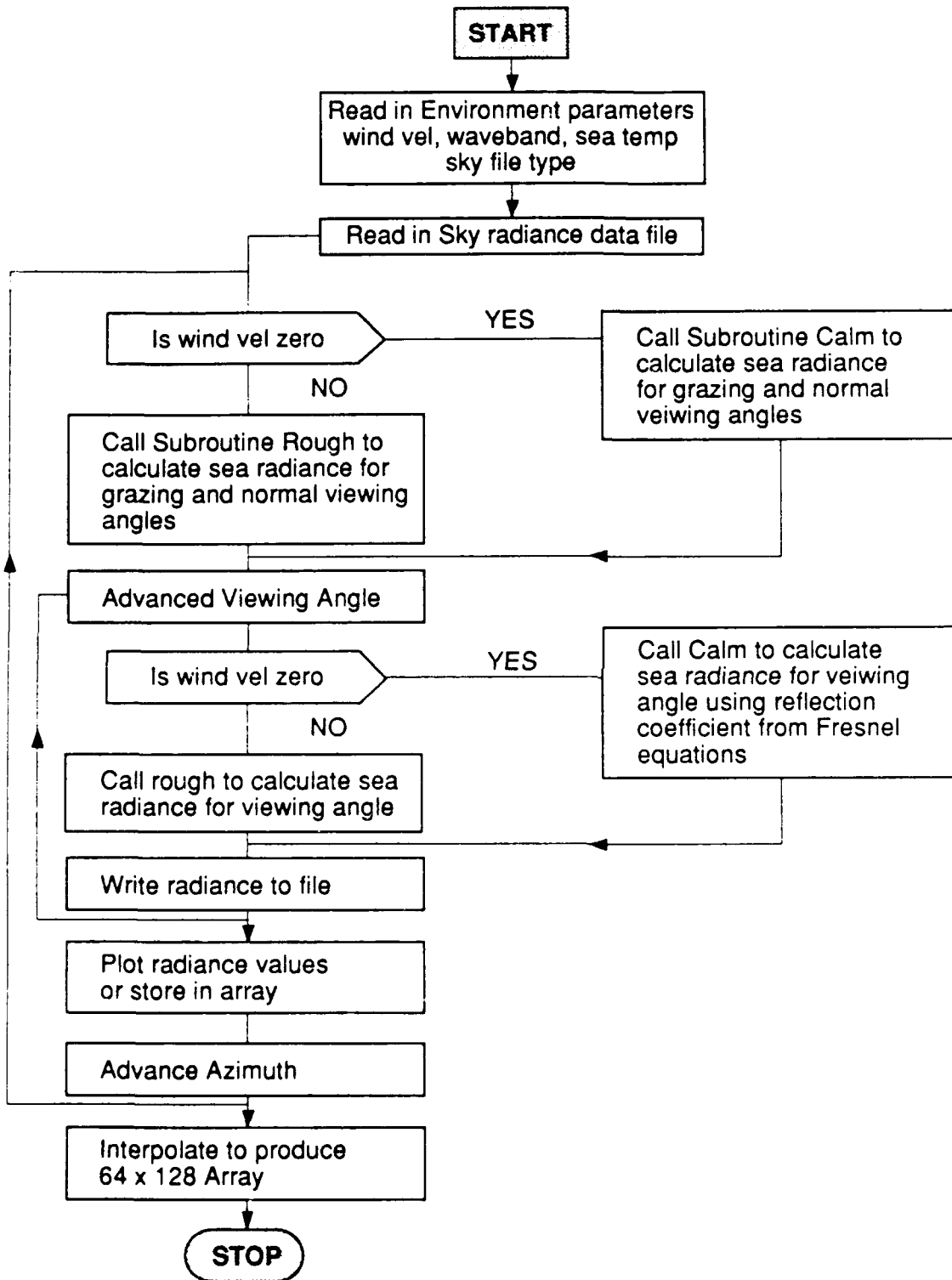


Figure 2(a). Flow diagram of radiance model main program

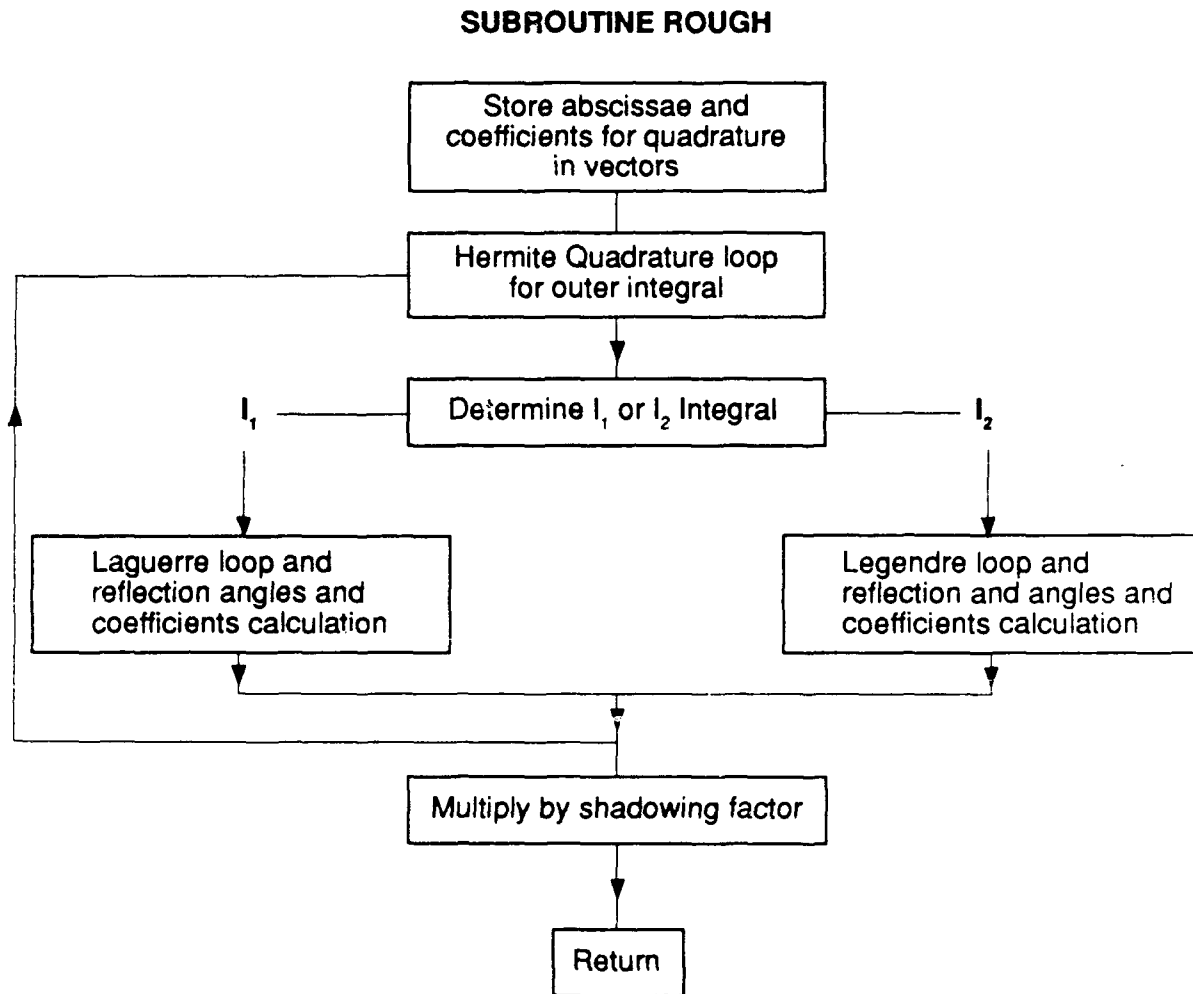


Figure 2(b). Flow diagram of subroutine rough

4. RESULTS AND DISCUSSIONS

4.1 Long waveband

To confirm the validity of the numerical technique used to read, interpolate and integrate within the model, comparison of the sea radiance from the model oceanrad was made in the 8.3 to 12.5 μm waveband against the values obtained by Saunders as shown in figures 3(a) and 3(b). Similarly in this waveband, some important conclusions must be commented on:

(i) As the 'look-down' angle (shown as negative angles) decreases from 90° to 45°, the sea becomes only fractionally cooler with only a small departure from the Black Body temperature of the sea. Even at 90° the sea radiance will always be smaller than that of a Black body since its reflectivity is always greater than zero.

(ii) Except for a condition of zero wind speed, the sea radiance decreases with the magnitude of the look down angle. The radiance at the horizon for each value of wind speed varies discontinuously to that of the sky above. The magnitude of discontinuity decreases for increasing wind speed hence sea roughness.

(iii) The calm sea exhibits no discontinuities at or near the horizon, however, the sea radiance, within an angle of 0.5° of the horizon, becomes increasingly hotter until it reaches the near ambient temperature of the horizon sky. Because the calm sea is flat, then for grazing look down angles, the warm horizon sky will be reflected to the observer. However, in the presence of waves and as a result of the Shadowing Factor S in equation (3), then the sea appears 'dish shaped'. That is for grazing look down angles the sea now has a non-zero slope probability $p(Z_x, Z_y)$ and the colder sky is reflected accordingly.

Figure 4 shows the mean radiance of the sea in the 8 to 12 μm waveband as a function of the refractive index. Because different authors have used different refractive indices for sea water (Cox and Munk 1.338, Saunders 1.237 and others which obtain a range of values between 1.334 to 1.36 depending upon the salinity and chlorinity content) a large variation of the sea radiance may result from differentiating indices. The three sets of curves in figures 4(a) and 4(b) represent the effect of wind speeds 1.36 ms^{-1} and 17 ms^{-1} which correspond to sea roughness of $\delta = 0.1$ and 0.3 respectively. Most variation in radiance occurs at grazing look down angles for both maximum and minimum velocities. Table 1 contains the numerical values of figures 4(a) and 4(b) for the largest and smallest values of refractive indices. The difference in radiance for such values can be seen at the bottom of the table indicating that an arbitrary choice of refractive index within the given range will result in a maximum variation in radiance of less than 5%. This percentage will decrease as the magnitude of the look down angle increases. It is therefore expected that an incorrect choice of the refractive index within the specified range will not significantly change the sea radiance.

4.2 Short waveband

As discussed earlier, the sky radiance in the short infrared waveband is a function of azimuth angle. The main contribution of angular dependence comes from direct and indirect (scattered) solar radiation. As shown in figure 5, elevation is plotted against mean sky radiance for five different azimuth angles.

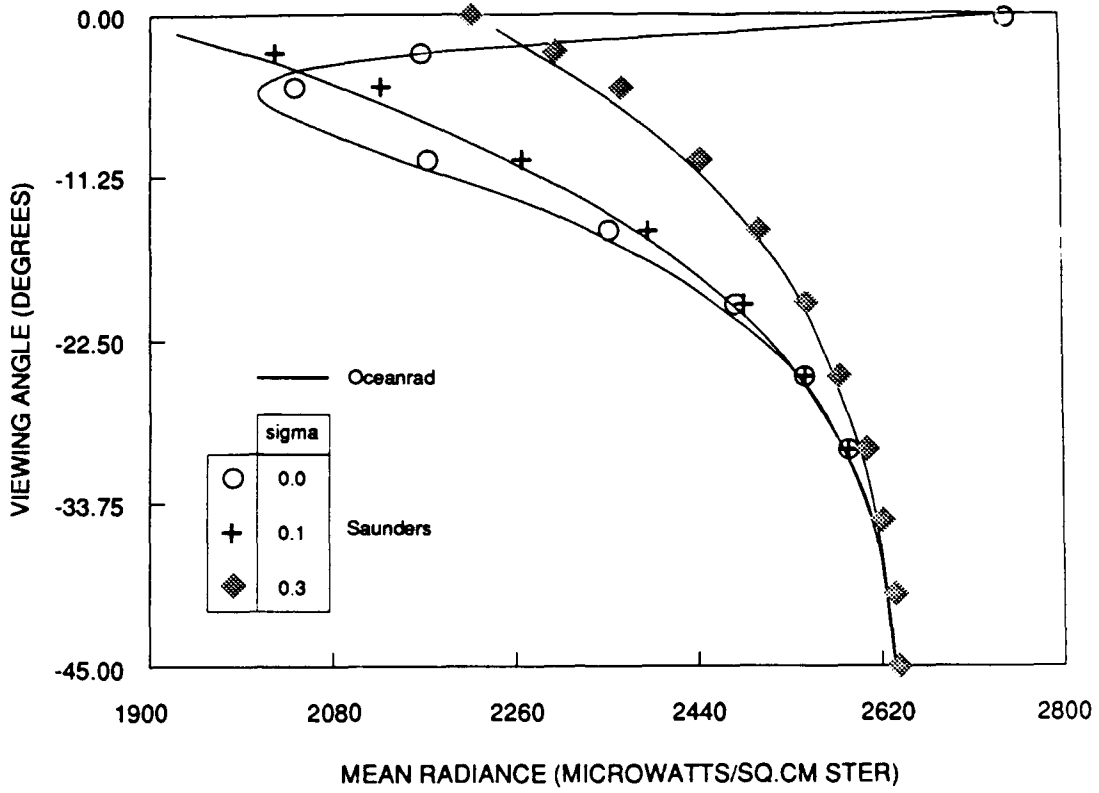


Figure 3(a). Comparative LWB sea radiance profiles

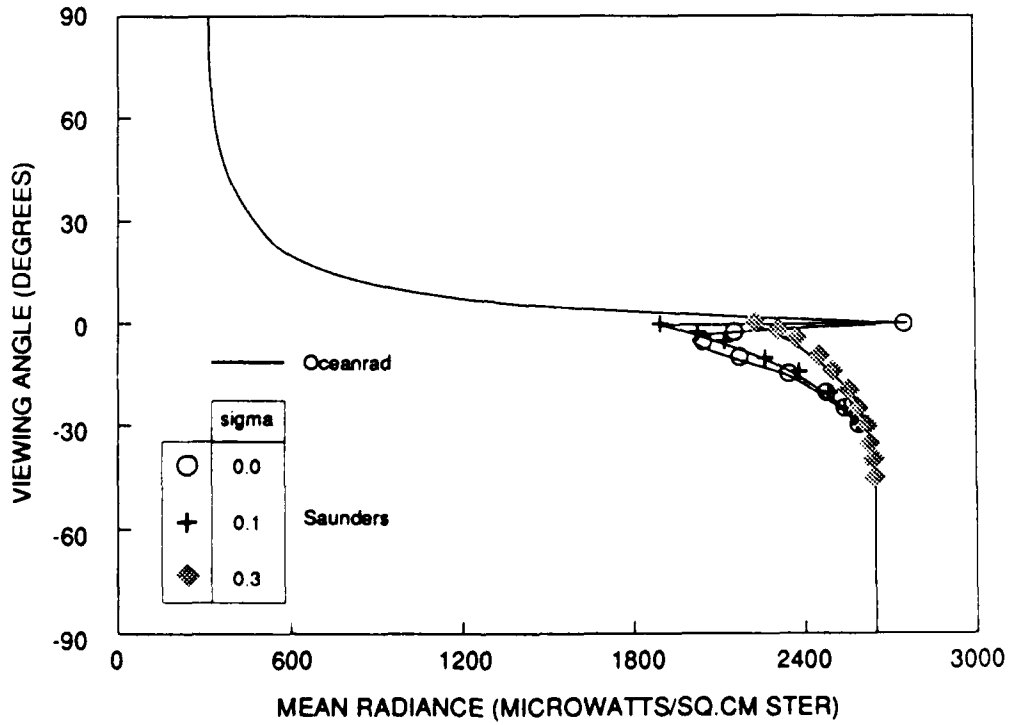


Figure 3(b). Comparative LWB sea/sky radiance profiles

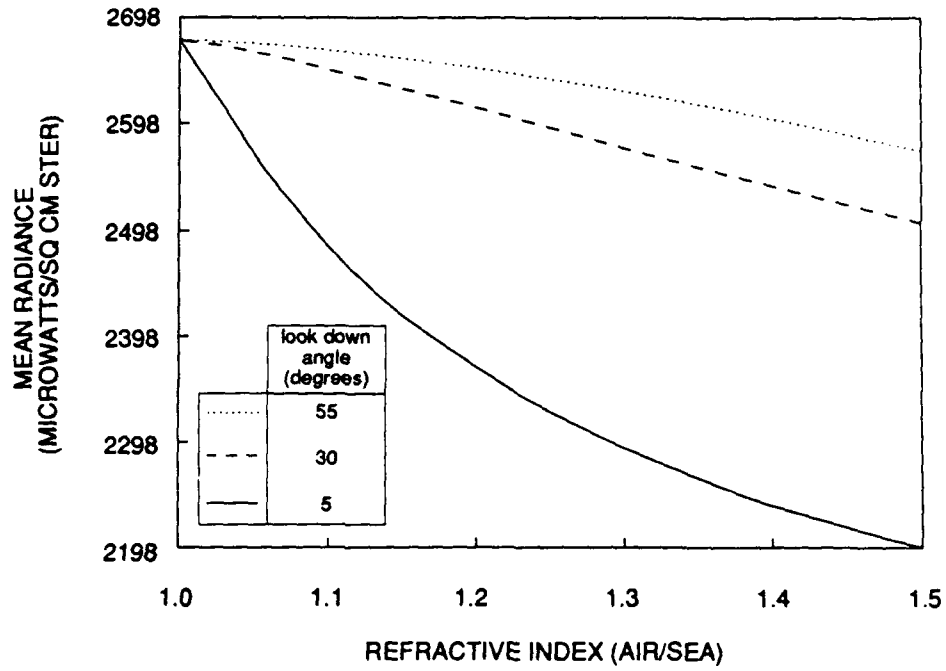


Figure 4(a). Mean radiance against refractive index for $\delta = 0.1$

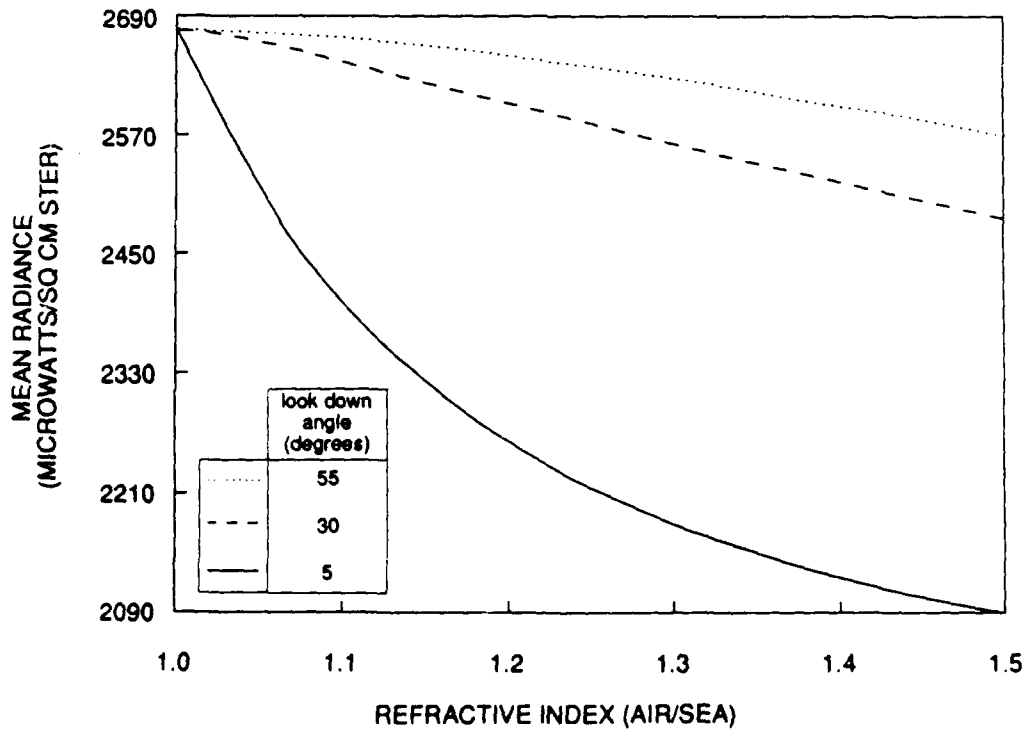


Figure 4(b). Mean radiance against refractive index for $\delta = 0.3$

TABLE 1. COMPARATIVE VARIATION IN SEA RADIANCE VALUES

Authors	Look down Angle								Refractive index
	2°		5°		30°		55°		
Saunders	1965	2267	2085	2333	2578	2598	2639	2639	1.240
Cox and Munk	1911	2200	2024	2269	2537	2562	2615	2616	1.338
Handbook	1902	2188	2015	2258	2528	2555	2610	2610	1.360
	63	79	70	75	50	43	29	29	ΔN

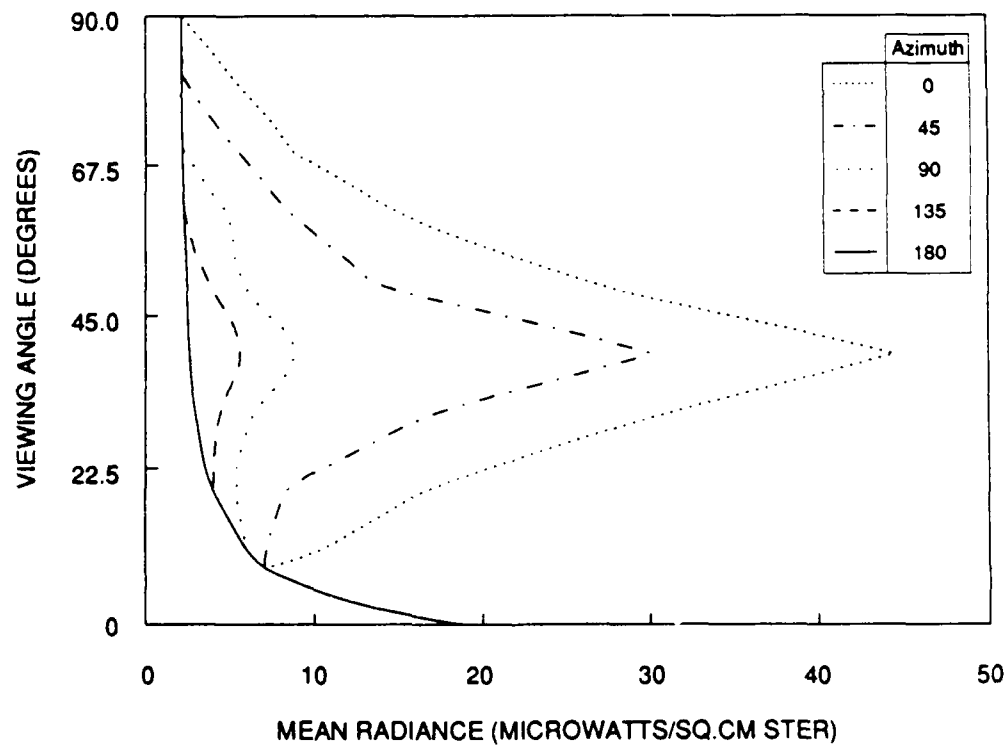


Figure 5. Elevation as a function of mean sky radiance SWB

Such sky radiance only approximates the expected 3 to 4 μm radiance map, since it is the purpose of this report to present a model and not to present a comparative assessment between measured and numerically calculated infrared radiance maps. As shown by the increase in radiance, the sun is approximately 43° in the east.

Figure 6(a) shows both the sea and sky radiance as a function of 'look down angle' for an azimuth direction of 180° (directly away from the sun) and figure 6(b) shows the radiance for an azimuth direction of 0° .

In each figure the two curves represent the calculated radiance for a wind velocity of 0 and 20 ms^{-1} . The radiance curve in figure 6(b) for 0 ms^{-1} is similar to the LWB results 'in trend' in that the values decrease as depression decreases to a value at -5° then rises sharply at the horizon. However, it does contain the additional radiance of scattered sun radiance which can be seen reflected in the sea at -43° . The intensity from such a reflection is reduced as expected from the increased emissivity of the sea for that angle.

For sea state or roughness other than $\delta = 0$, the short waveband radiance-profile can differ significantly from that of the long waveband. As shown in figure 6(b) (depending upon sun elevation), a situation can be attained where the radiance remains constant or may even increase toward the horizon. This results in the discontinuity for the sea/sky interface either not being present or inverted to that which is usually expected.

Figure 7 represents radiance profiles for wind velocities of 20 ms^{-1} for a number of different azimuth angles. This demonstrates the totally different sea signatures which can be achieved depending upon the observed azimuth angles. Notice that for look down angles with a magnitude greater than 45° the radiance of the sea approaches that of a 'black body'.

4.3 Image representation

The data output from the sea radiance model was written into a data file of 37 columns and 64 rows. Using two dimensional linear interpolation, a second data file of 128 columns and 64 rows was generated. In this format the radiance information could be coded and displayed on a PC (16 bit Amiga) using an identical 'grey scale' display as that which the Aga Thermavision Thermal Imager formats. At present the coding is such that the grey scale is limited to 11 levels for display purposes.

For a single azimuth angle, the radiance program takes 10 s to run for a zero input wind speed, and 90 s for any finite wind speed other than zero. Numerically generated radiance images of the maritime scene using the sea radiance program and the long and short waveband (LWB and SWB) are shown in figures 8 and 9. Each image results from the observer subtending a 60° field of view. The horizon in each case occurs at the midpoint of the vertical field of view.

In particular, figure 8(a) shows the 8 to 12 μm (LWB) image for a wind speed of zero (left hand image), and 5 ms^{-1} (right hand image). In each picture, and to the extreme right, a grey scale of 11 levels is displayed. 'Hotter regions' are characterised by a 'lighter' level of grey scale. The horizon separating the colder sky from the warmer sea can be clearly distinguished.

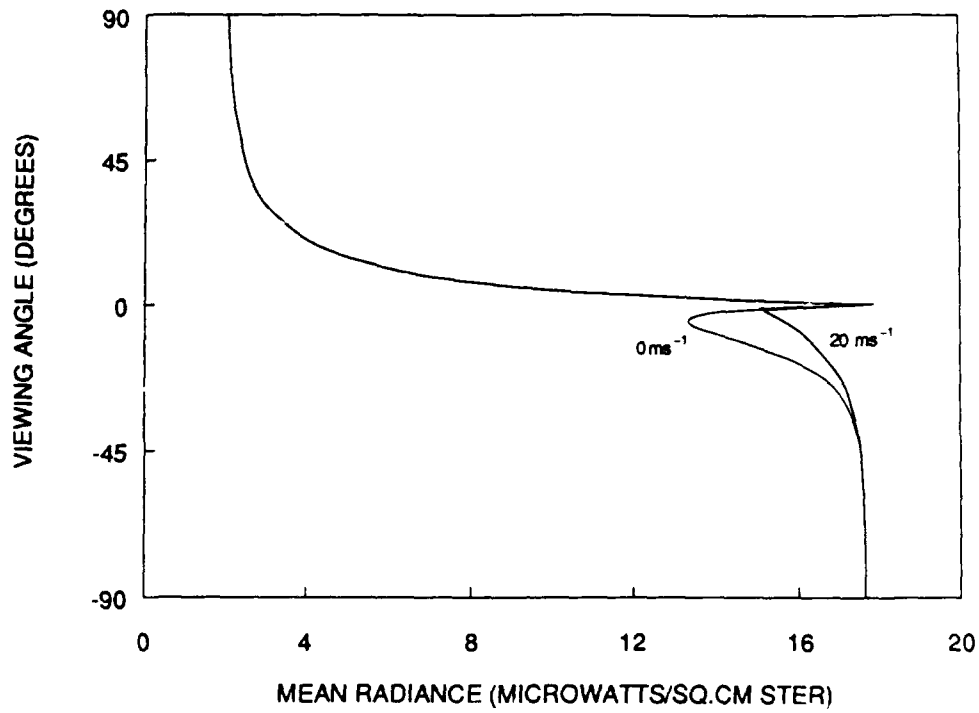


Figure 6(a). SWB sea/sky radiance profile for 180° azimuth angle from sun

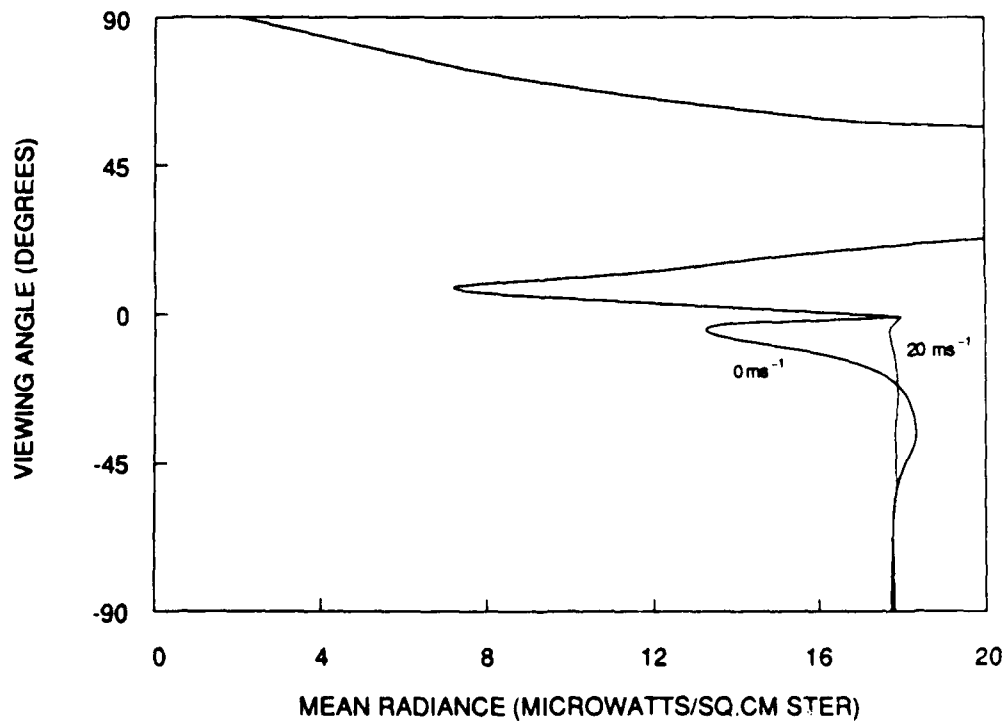


Figure 6(b). SWB sea/sky radiance profile for same sun azimuth angle

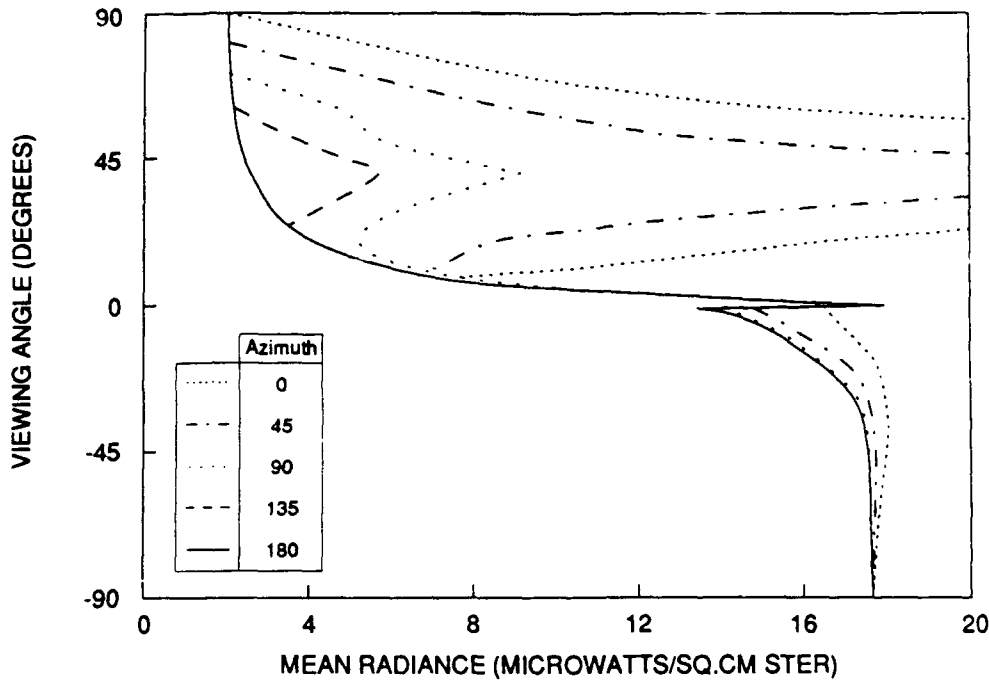


Figure 7. SWB sea/sky radiance profile for different azimuth angles

Figure 8(b) shows the numerical model of a Guided Missile Destroyer inserted onto the LWB sea background. The grey scale of the target at this stage is not meant to be compatible to its background since such an image is included to only demonstrate an example of an application of the sea radiance imaging facility.

The left picture of figure 9(a) represents the 8 to 12 μm (LWB) image which can be compared to the right picture which represents the SWB image of the maritime scene for a common wind velocity of zero. The azimuth dependence of the radiance can be clearly seen for the SWB. Figure 9(b) shows the effects of different wind speeds of zero and 5 ms⁻¹ for the SWB image. Again variation in radiance is evident as a function of both wind speed and azimuth direction.

4.4 Irradiance

Once the radiance of the sea surface has been determined, the incident power of the electromagnetic energy (irradiance) at a unit surface on the observer's optics can be determined. If the range between the emitting sea and observer is sufficiently large (at wavelengths corresponding to the atmospheric windows) or if wavelengths within the absorption profiles of the atmosphere are considered then effects from the intervening atmosphere must be account for. This is considered in the following irradiance equation which is given by:

$$H(\lambda, \phi) = \frac{A}{R^2} [N(\phi) \tau(\lambda) + N_A(\phi, R)] \tag{7}$$

where $N(\phi)$ corresponds to the sea radiance as given by equation (3) and $N_A(\phi, R)$ is the total radiance of the intervening atmosphere. It must also be noted that the irradiance is more accurately the spectral irradiance, although in the atmospheric windows, $\tau(\lambda)$ the atmospheric transmittance, is very nearly constant. However if τ is a function of the wavelength and appreciably changes over the waveband of detectability, then the observed irradiance is given by

$$H(\phi) = \frac{1}{\Delta\lambda} \int_{\lambda_1}^{\lambda_2} H(\lambda, \phi) D(\lambda) d\lambda$$

where $\Delta\lambda = \lambda_2 - \lambda_1$ and represents the waveband in which the observation is made. The term $D(\lambda)$ accounts for the transmittance for the spectral passband of the detector.

The term in parenthesis in equation (7) differs from the sea radiance $N(\phi)$ with a magnitude which depends upon both the atmospheric transmittance $\tau(\lambda)$ and the airlight emission radiance $N_A(\lambda)$. Therefore, in the 3 to 4 μm and 8 to 12 μm waveband, effective sea temperatures can differ significantly from the actual combined sea/sky temperatures for the same look down angle. This may well be of significance for a weapon imaging system tracking a target at or near the horizon.

Figure 10 shows an optical surveillance system relative to the horizon, where r is the earth's radius, s is the vertical height of the observer, L_m is the distance from the observer to the horizon and L_2 is the line of sight to the sea surface which makes an angle μ to the vertical. From the simple geometry, the angle from the vertical to L_m is given by:

$$\phi = \sin^{-1} \left(\frac{r}{r+s} \right)$$

hence

$$L_m = r \cot \phi$$

and using the cosine law for triangles, and simplifying, L_2 is given by:

$$L_2 = (r+s) \cos \mu - \{r^2 - \sin^2 \mu (r+s)^2\}^{1/2}$$

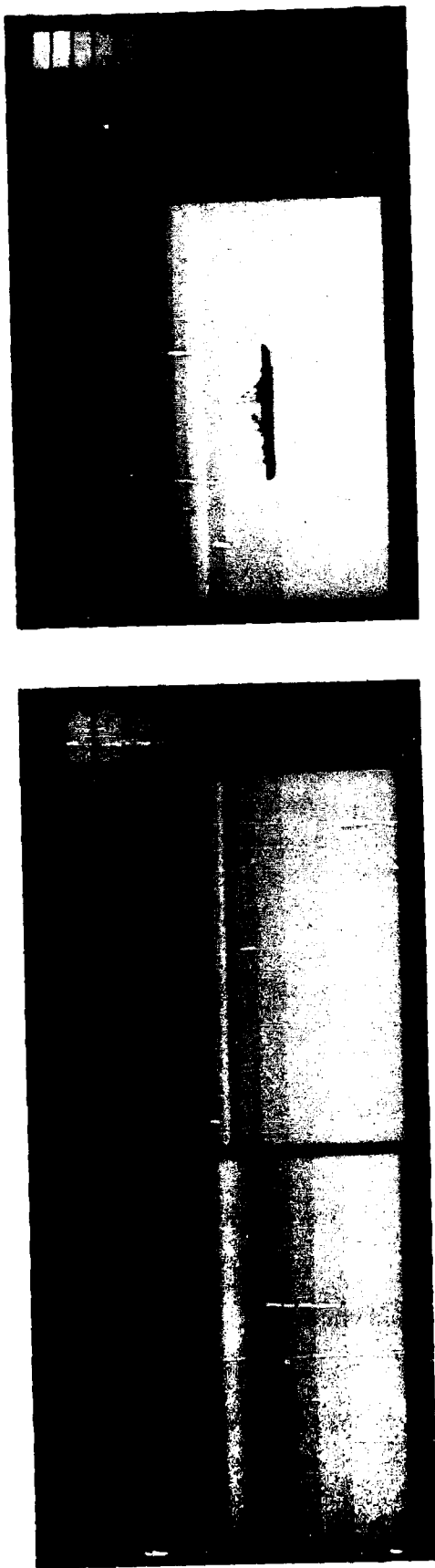


Figure 8. Numerical generation of (LWB) 8 to 12 μm images of the maritime scene

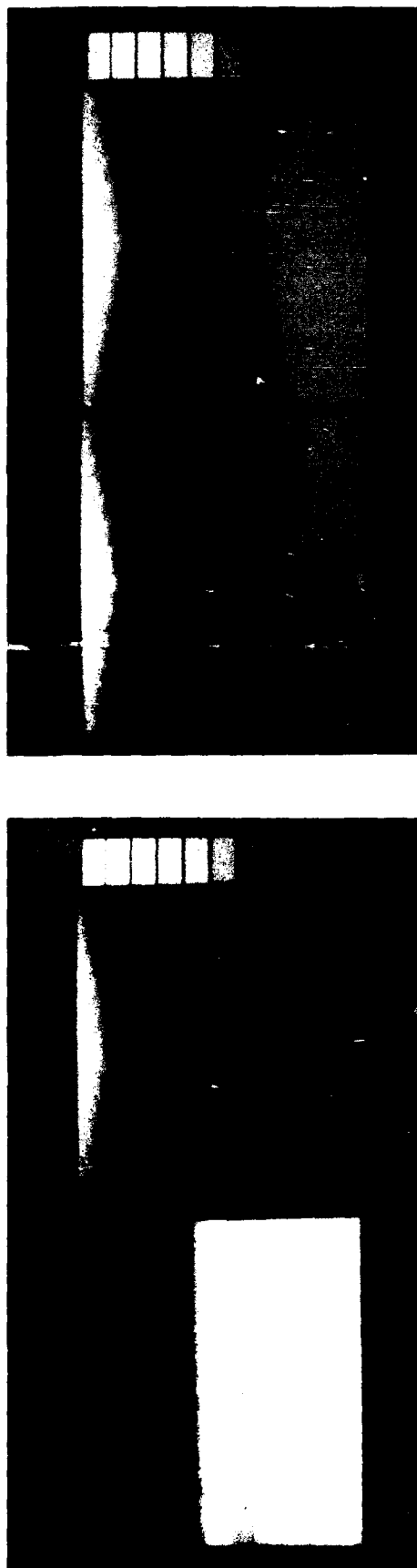


Figure 9. Numerical generation of LWB and (SWB) 3 to 4 μm images of the maritime scene

Figure 11 shows a plot of L_2 as a function of viewing angle μ , for altitudes (s) of 10 m and 1000 m respectively. For an observers at 10 m, a look down angle to the horizon gives an L_2 of 272 m. The average atmospheric transmission for this range is 0.91^1 so that the horizon contrast will still be clearly distinguished. However, at an altitude of 1 km, even though the decrease in path length as a function of look down angle, is substantial, for $\mu = 75.5^\circ$ $L_2 = 4.0$ km which corresponds to a transmissivity of only 0.25. Therefore, depending upon the atmospheric conditions and observers height above sea level there may be very little or no discernable contrast between the sky and sea, furthermore the sea may appear a uniform temperature for all look down angles.

To find those look down angles which give significant atmospheric dependent irradiance values, we can choose a value of 2 km as the critical path length such that in a maritime midlatitude summer environment, the atmospheric transmission is between 0.5 and 0.6. A plot of look down angle as a function of vertical height can be determined and is shown in figure 12. Values above the curve indicate vertical heights and associated look down angles where the airlight can contribute significantly to the irradiance at the observer for both the 8 to 14 μm and 3 to 4 μm atmospheric windows.

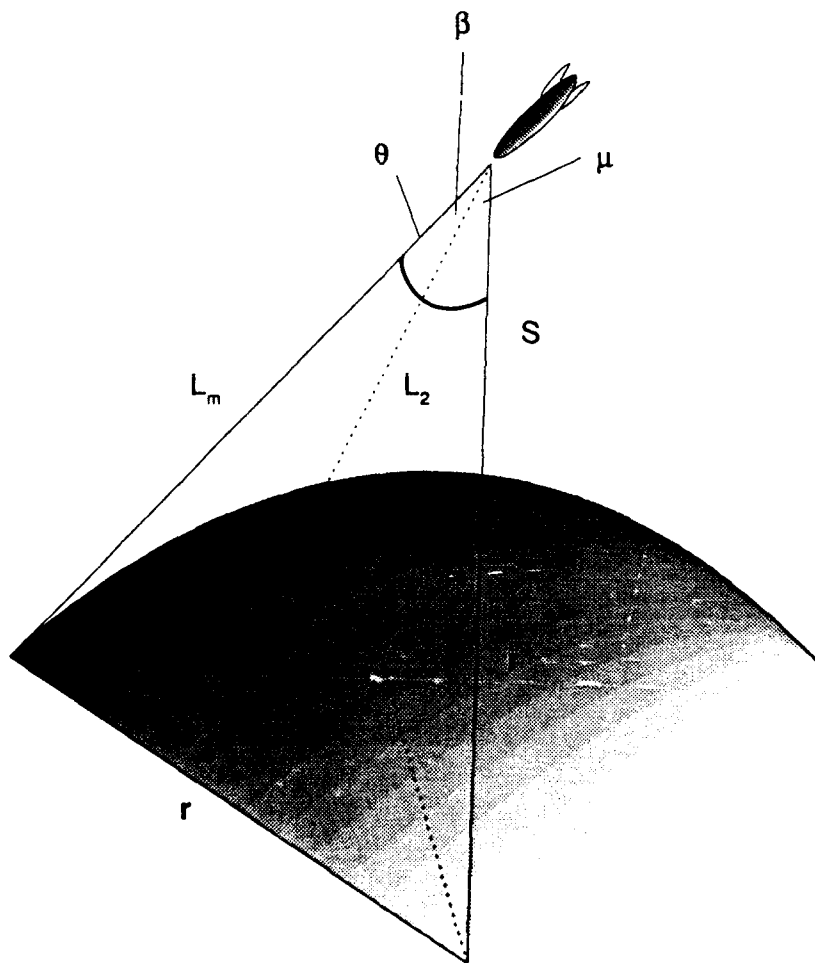


Figure 10. Geometry of observer relative to the Earth horizon coordinate system

¹ The transmission figures were obtained from Lowtran 6 for the 8 to 12 μm waveband.

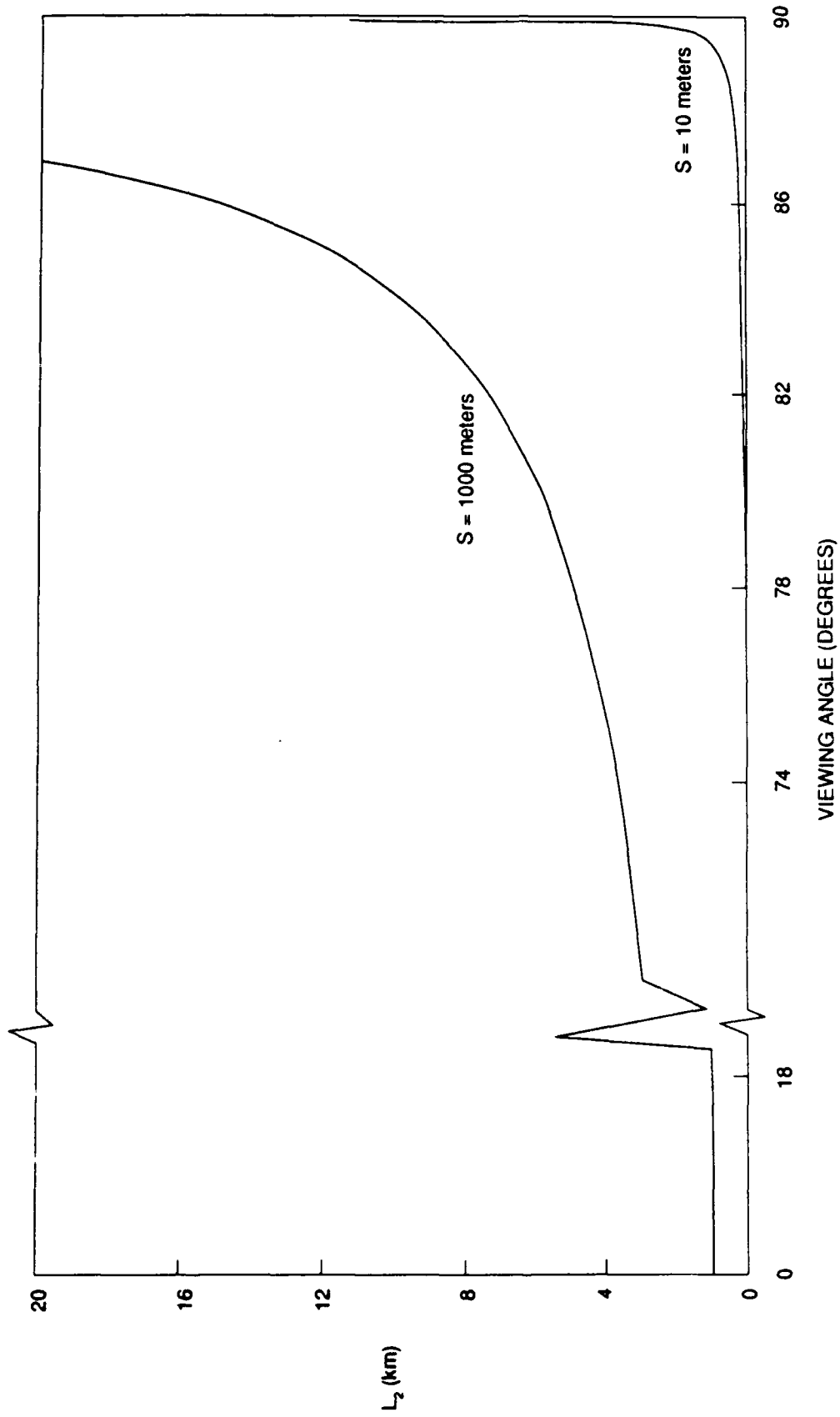


Figure 11. L_2 as a function of viewing angle

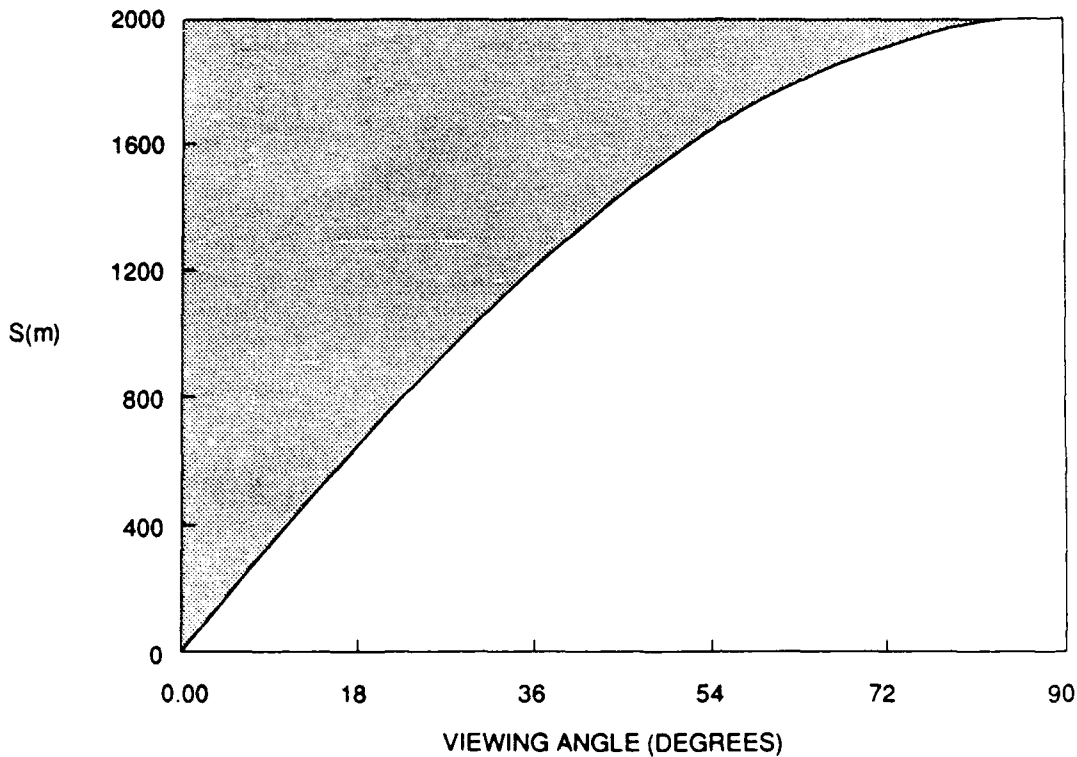


Figure 12. Vertical height as a function of viewing angle

5. CONCLUSION

The statistical infrared signature model for both a calm and wind roughened sea enables a relatively simple and fast numerical technique to calculate sea radiance values to produce data which can be further used in processing routines incorporated within weapon or surveillance system algorithms. A further comparison of calculated and experimental measured sea irradiances for different wavebands and sea states needs to be made for a higher degree of validity between the model and a true maritime environment.

Using Quadrature was one way of numerically evaluating the otherwise awkward integrals. When there is a high degree of variation in the sky radiance, such as broken cloud cover, then successively higher point Quadrature must be used if the same numerical accuracy is required.

This then may not become the most time efficient integral solving technique and an alternative integral evaluation method should be sought.

6. ACKNOWLEDGEMENTS

The authors wish to thank Mr R. Rossiter and Mr D. Najar for their assistance in coding and data processing to produce the radiance and image profiles. Thanks also go to Mr O. Scott for many useful discussions.

REFERENCES

- | No. | Author | Title |
|-----|-----------------------------------|---|
| 1 | Saunders, P.M. | "Radiance of Sea in the Infrared Window 800 to 1200 cm^{-1} ".
Journal of the Optical Society of America,
Vol 58, No 5, p645, 1986 |
| 2 | Brunker, S. | "A Proposed Geometrical Method to Model the Time Varying Infrared Signature of a Wind-Roughened Sea".
To be published |
| 3 | Cox, C. and
Munk, W. | "Measurement of the Roughness of the Sea Surface from Photographs of the Sun's Glitter".
Journal of the Optical Society of America,
Vol 49, No 11, p838, 1954 |
| 4 | Wilf, I. and
Manor, Y. | "Simulation of Sea Surface Images in the Infrared".
Applied Optics, Vol 23, No 18, p3174, 1984 |
| 5 | Chapman, R. and
Irani, G. | "Errors in Estimating Slope Spectra from Wave Images".
Applied Optics, Vol 20, No 20, p3645, 1981 |
| 6 | Editor Weast, R. and
Astle, M. | "CRC Handbook of Chemistry and Physics".
59th edition D-296, 1978 to 1979 |

APPENDIX I

REFLECTED ANGLE DETERMINATION

The geometry of reflection of the 'sky' off a wave facet to the observer is shown in figure 1. α is the angle made between the observer and the y axis, in the y z plane. The facet has a maximum slope β at an azimuth direction α taken from the y axis. By the law of reciprocity, the reflected ray has polar coordinates ν and μ where the angle between the observer and reflected sight line is give by ω .

To find an expression for the component of the maximum slope in terms of maximum slope polar coordinates, then consider figure I.1 which represents a cartesian surface. The equation of the tangent plane at a point 'a' on the surface having coordinates (X_0, Y_0, Z_0) is given by

$$Z = Z_0 + (x - x_0) \frac{\partial f}{\partial x} + (Y - Y_0) \frac{\partial f}{\partial Y} \quad (I.1)$$

where the normal vector at 'a' is

$$\left(\frac{-\partial f}{\partial x}, \frac{-\partial f}{\partial Y}, 1 \right)$$

If point 'a' becomes the coordinate system's origin, then equation (I.1) reduces to:

$$Z = Z_0 + X \frac{\partial f}{\partial x} + Y \frac{\partial f}{\partial Y} \quad (I.2)$$

Since $\text{grad } Z$ gives the (x, y) coordinates of the maximum gradient vectors on the tangent surface, then the above equation becomes:

$$Z = \left(\frac{\partial f}{\partial x} \right)^2 + \left(\frac{\partial f}{\partial Y} \right)^2$$

But

$$Z = R \tan \beta$$

and since

$$R^2 = \left(\frac{\partial f}{\partial x}\right)^2 + \left(\frac{\partial f}{\partial y}\right)^2$$

then

$$R = \tan \beta$$

Also, any vector which has a maximum slope, has coordinates given by $x = R \sin \alpha$ and $y = R \cos \alpha$

therefore

$$\begin{aligned} \sin \alpha \tan \beta &= \frac{\partial f}{\partial x} \\ &= Z_x \end{aligned}$$

and

$$\cos \alpha \tan \beta = Z_y$$

where

$$\tan^2 \beta = Z_x^2 + Z_y^2$$

thus given Z_x and Z_y , β and α can be determined.

The reflection angles ν and μ are given by the following equations, the derivation of which can be found in reference 1.

$$\cos \omega = \cos \beta \sin \phi - \cos \alpha \sin \beta \cos \phi$$

$$\cos \mu = 2 \cos \beta \cos \omega - \sin \phi$$

$$\cot \nu = \cot \alpha + \frac{1}{2} \csc \alpha \csc \beta \sec \omega \cos \phi \quad (1.3)$$

The sign of the second term in equation (I.3) is however opposite to that obtained by Cox and Munk in reference 3.

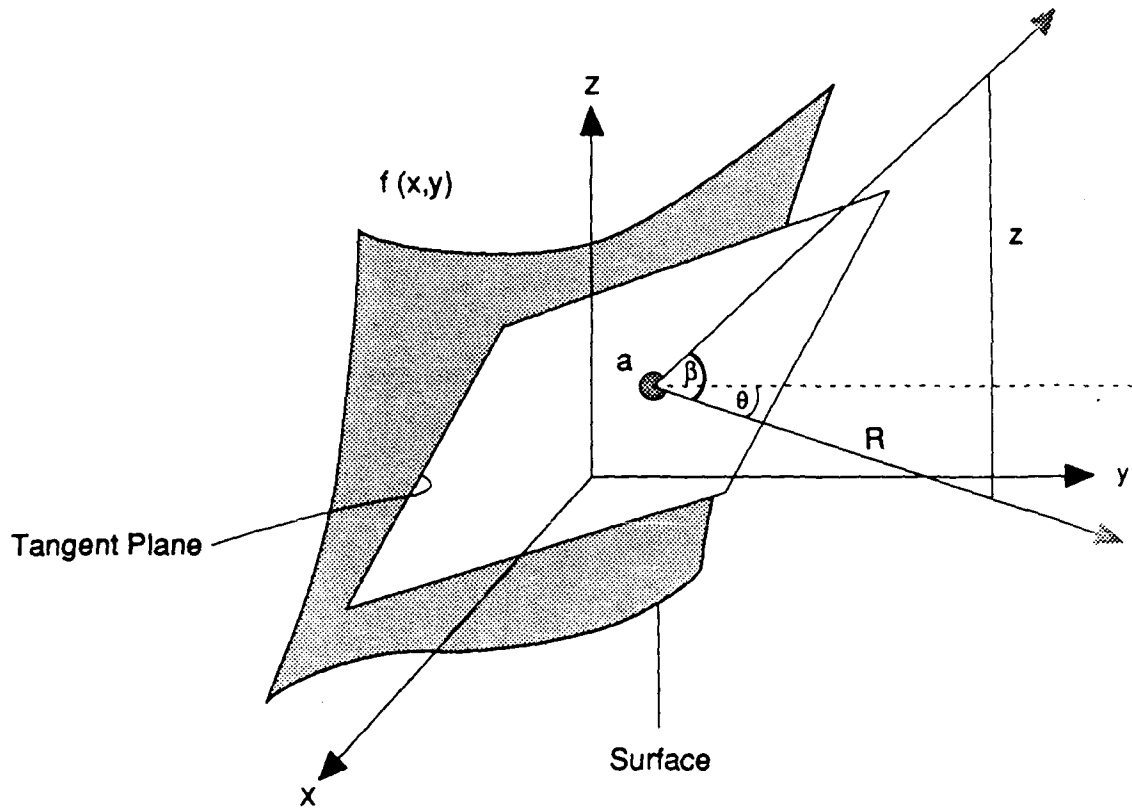


Figure I.1 Wave facet as tangent plane

APPENDIX II

SEA RADIANCE INTEGRAL EVALUATION

Given the azimuth and elevation angles (α, ϕ) of the observer, the sea radiance integral is given by

$$N(\alpha, \phi) = \frac{S}{\pi \delta^2} \int_{-\infty}^{\infty} \int_{-\infty}^{\tan \phi} [B - R[B - NS]] \cos \omega \sec \beta \exp \left[-\frac{(Z_x^2 + Z_y^2)}{\delta^2} \right] dZ_x dZ_y$$

where S is the shadow factor. The radiance expression in the above integral can be represented by a function $F(Z_x, Z_y)$ such that:

$$F(Z_x, Z_y) = [B - R[B - NS]] \cos \omega \sec \beta$$

so the integral reduces to:

$$N(\alpha, \phi) = \frac{S}{\pi \delta^2} [I_1 + I_2]$$

where

$$I_1 = \int_{-\infty}^{\infty} \int_{-\infty}^0 F(Z_x, Z_y) \exp \left[-\frac{(Z_x^2 + Z_y^2)}{\delta^2} \right] dZ_x dZ_y$$

and

$$I_2 = \int_{-\infty}^{\infty} \int_0^{\tan \phi} F(Z_x, Z_y) \exp \left[-\frac{(Z_x^2 + Z_y^2)}{\delta^2} \right] dZ_x dZ_y$$

By a change of variables the integrals I_1 and I_2 can be evaluated using Gauss Quadrature as follows.

II.1 Change of variables for I

letting

$$\gamma = \frac{Z_x}{\delta}$$

and

$$\psi = \frac{Z_y}{\delta}$$

Then

$$I_1 = \delta^2 \int_{-\infty}^{\infty} \left[\int_{-0}^{\infty} G(\gamma, \psi) e^{-\psi} d\psi \right] e^{-\gamma^2} d\gamma$$

where

$$G(\gamma, \psi) = F(\delta\gamma, \delta(-\psi)) e^{\psi - (-\psi)^2}$$

II.2 Change of variables for I₂

by letting

$$\gamma = \frac{Z_x}{\delta}$$

and

$$\rho = \frac{2\frac{Z_y}{\delta} - \epsilon}{\epsilon}$$

where

$$\epsilon = \frac{\tan \phi}{2}$$

then

$$I_2 = \delta^2 \int_{-\infty}^{\infty} \left[\epsilon \int_{-1}^1 F(\gamma\delta, \delta(\epsilon + \rho\epsilon)) \exp - (\epsilon + \rho\epsilon)^2 d\rho \right] e^{-\gamma^2} d\gamma$$

DISTRIBUTION

No. of copies

DEPARTMENT OF DEFENCE

Defence Science and Technology Organisation

Chief Defence Scientist

First Assistant Secretary Science Policy

First Assistant Secretary Science Corporate Management

Counsellor, Defence Science, London

Counsellor, Defence Science, Washington

Counsellor, Defence Science, Bangkok

Defence Adviser, Defence Research Centre, Kuala Lumpur

}
} 1
}

Cnt Sht Only

Cnt Sht Only

Cnt Sht Only

Cnt Sht Only

Electronics Research Laboratory

Director, Electronics Research Laboratory

Chief, Electronic Warfare Division

Senior Principal Research Scientist, Electronic Warfare Division

Head, Optical Electronic Warfare Group

Head, Optical Development Group

Head, Electronic Warfare Techniques Group

Dr S.S. Ti, Optical Electronic Warfare Group

Mr O.S. Scott, Optical Electronic Warfare Group

Mr R.J. Oermann, Optical Electronic Warfare Group

1

1

1

1

1

1

1

1

1

Materials Research Laboratories

Director, Materials Research Laboratories

Chief, Physics Division

1

1

Surveillance Research Laboratory	
Chief, Optoelectronics Division	1
Head, Systems Analysis Group	1
Dr G. Burfield, Systems Analysis Group	1
Weapons Systems Research Laboratory	
Director, Weapons Systems Reserach Laboratory	1
Navy Office	
Navy Scientific Adviser	Cnt Sht Only
Director, Research Requirements	1
Army Office	
Scientific Adviser - Army	1
Air Office	
Air Force Scientific Adviser	1
Joint Intelligence Organisation (DSTI)	1
Libraries and Information Services	
Librarian, Technical Reports Centre, Defence Central Library, Campbell Park	1
Document Exchange Centre	
Defence Information Services Branch for:	
Microfiche copying	1
United Kingdom, Defence Research Information Centre	2
United States, Defense Technical Information Center	12
Canada, Director, Scientific Information Services	1
New Zealand, Ministry of Defence	1
National Library of Australia	1

Main Library, Defence Science and Technology Organisation Salisbury	2
Library, Aeronautical Research Laboratories	1
Library, Materials Research Laboratories	1
Library, Aircraft Research and Development Unit	1
Library, DSD, Melbourne	1
Defence Industry and Materiel Policy Division	
FASDIMP	1
THE TECHNICAL COOPERATION PROGRAM (TTCP)	
Australian National Leader Subgroup Q (Attention: Executive Chairman)	3
Australian National Leader QTP-10	
UK National Leader	1
US National Leader	1
Canada National Leader	4
NZ National Leader	1
PRIVATE ENTERPRISE	
British Aerospace, Technology Park, SA	4
Fairey Australasia, Holden Hill, SA	1
UNITED KINGDOM	
British Library, Document Supply Centre (UK)	1
Author	4
Spares	4
Total number of copies	70

DOCUMENT CONTROL DATA SHEET

Security classification of this page :

UNCLASSIFIED

1 DOCUMENT NUMBERS

AR
Number: AR-005-879

Series
Number: ERL-0473-TR

Other
Numbers:

2 SECURITY CLASSIFICATION

a. Complete Document: Unclassified

b. Title in Isolation: Unclassified

c. Summary in Isolation: Unclassified

3 DOWNGRADING / DELIMITING INSTRUCTIONS

4 TITLE

A STATISTICAL MODEL OF THE INFRARED SIGNATURE OF A WIND ROUGHENED SEA

5 PERSONAL AUTHOR (S)

S.A. Brunker and
G. Hamlyn

6 DOCUMENT DATE

March 1989

7 7.1 TOTAL NUMBER OF PAGES

28

7.2 NUMBER OF REFERENCES

6

8 8.1 CORPORATE AUTHOR (S)

Electronics Research Laboratory

9 REFERENCE NUMBERS

a. Task: Associated: DIR 88/009

b. Sponsoring Agency:

8.2 DOCUMENT SERIES and NUMBER

Technical Report
0473

10 COST CODE

233

11 IMPRINT (Publishing organisation)

Defence Science and Technology
Organisation Salisbury

12 COMPUTER PROGRAM (S)
(Title (s) and language (s))

13 RELEASE LIMITATIONS (of the document)

Approved for Public Release

Security classification of this page :

UNCLASSIFIED

14 ANNOUNCEMENT LIMITATIONS (of the information on these pages)

No limitation

15 DESCRIPTORS**a. EJC Thesaurus
Terms**

Infrared signatures
 Mathematical models
 Sea surface effects detection
 Wind effects

**b. Non - Thesaurus
Terms****16 COSATI CODES**

0063C
 0047B

17 SUMMARY OR ABSTRACT

(if this is security classified, the announcement of this report will be similarly classified)

The response of any Optical System, used in either a weapon or surveillance mode, is dependent upon the emission of electromagnetic energy from both target and background occupying the field of view. The background not only contributes to the infrared scene (clutter) but, additionally, by reflection and absorption, can significantly contribute to the target's signature.

Since the maritime environment can be conceived as containing an opaque homogeneous body of water, its signature will depend upon the predictable behaviour of such a surface in response to the natural elements.

This report proposes a statistical-numerical method which can be used to obtain the infrared signature of both a calm and wind roughened sea in the 1 to 5 μm waveband.